Interlayer Transport Measurement of Organic Ultrathin Film Using Microfluidic Channel Technology

Takamasa Hamai, Yuki Okamoto

Authors Information

Takamasa Hamai Department of applied Physics, Hasegawa-Arai laboratory. Specialty is organic single crystalline thin film transistors. In this study, he flowed liquid metal into micro channel and measured electrical characteristics.

Yuki Okamoto received his B.S. and M.S. degrees in electrical engineering in 2015 and 2017 from the University of Tokyo, and now is a Ph.D. student at the University of Tokyo. He is also a JSPS research fellow for Young Scientists. He is now working on CMOS-LSI integrated MEMS and microfluidics.

1. Introduction

The effect of interlayer transport in the device characteristics of organic thin film transistors

Organic semiconductor (OSC) molecules substituted by long alkyl chain are promising material for low-cost Thin-film transistor (TFT) fabrication because they can be fabricated in low-temperature and ambient pressure condition. Recently, Hasegawa-Arai laboratory succeeded in fabricating single crystalline, and millimeter-scale thin films of 2-decyl-7-phenyl[1]benzothieno[3,2-b][1]benzothiophene (Ph-BTBT-C10), which shows high mobility as 10 cm^2/Vs. Also we enabled the control of film thickness in the unit of molecular bilayer, and revealed that the alkyl chains, which improved the solubility and crystallinity, acted as insulating layers in the active layer of TFT to degrade device characteristics due to the tunneling-based nonlinear resistance [1]. Alkyl chain length is expected to be a control parameter not only of processability [2] but also carrier mobility. To obtain new high performance OSC, we need to simultaneously optimize processability, interlayer transport characteristics (mobility), and interlayer transport characteristics. A new method for direct measurement of interlayer transport in organic ultrathin films offers fundamental understanding of device

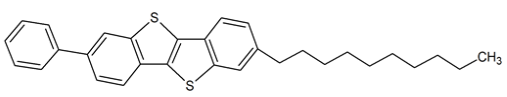

Fig. 1 Molecuar structure of Ph-BTBT-C10

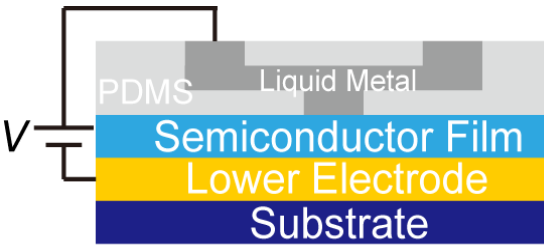

Fig. 2 Schematic of proposed device

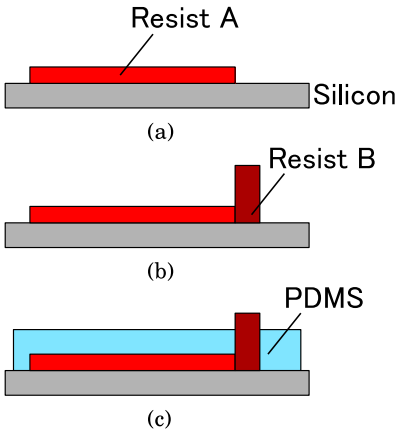

Figure 3. Process flow of the bottom layer of 3D liquid metal microfluidics in the previous study [4]. (a) The photoresist is patterned for the bottom channel. (b) The thicker photoresist is patterned for the fluidic via. (c) PDMS is spin-coated and cured.

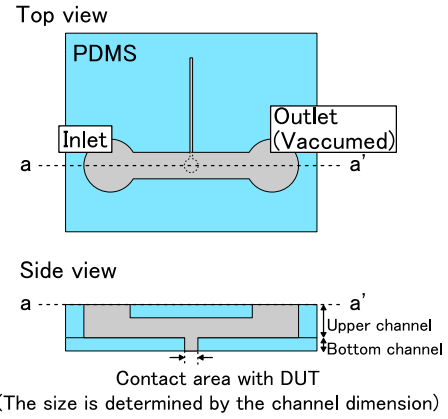

Figure 4. Schematic of liquid metal microfluidics in the previous study [4]. Degas is performed from the outlet and then the liquid metal is introduced from the inlet. Due to the liquid metal, the measurement can be performed invasively. The size contact area between the liquid metal and a DUT is determined by the size of the bottom micro channel.

degradation due to alkyl chain layers, and feedback to material design. However, interlayer transport measurement of ultrathin organic films (5 nm in minimum) is extremely difficult, because organic film can easily get damaged mechanically. So this kind of measurement on OSC molecules for TFT has not been reported. In metal evaporation process, which is generally used for electrode fabrication of organic TFT, evaporated metal atom thermally damage, and penetrate organic thin films [3]. To perform interlayer transport measurement, we need to develop appropriate process to fabricate bottom and top electrode without damaging organic thin films. We conceived a device structure with liquid metal as top electrode not to damage organic films under electrode fabrication.

Three-Dimensional Structure in Microfluidics

Microfluidic channels are commonly made from polydimethylsiloxane (PDMS) and fabricated using one mold. However, when three-dimensional (3D) structures are required, the device is composed of some layers. Besides, the connecting via between the fluidic layers has to be fabricated. Figure 3x shows the process flow of the bottom micro-channel of liquid-metal microfluidics in the previous study [4]. Firstly, a thin photoresist is patterned on a silicon wafer. Then, the thicker photoresist is patterned to form the fluidic via. After that, the PDMS is spin-coated on the mold. The thickness of the PDMS is well controlled by the rotation speed and is the

middle height between the two resist patterns. Finally, the upper microfluidic layer is bonded on the bottom microfluidic layer by using O_2 plasma. Although this method allows us to form the 3D structure, the height of the bottom micro-channel depends on that of the fluidic via. In other words, the height difference between the via and the bottom channel cannot be increased. As a result, if the rotation speed is a bit slower, PDMS covers even the fluidic via. On the contrary if the rotation speed is faster, the bottom channel is not completely covered and the microfluidic is not formed. Therefore, this method makes the yields of the fabrication worse.

2. Purpose

We have two purposes in this research: One is proposing a new non-invasive measuring method of organic ultrathin devices, and the other is optimization of microfluidics structure for liquid metal. We form non-invasive electrode by flowing liquid metal (eutectic gallium indium: EGaIn) into microfluidic channel. Utilizing the microfluidics technologies enables us to measure a device under test (DUT) keeping the constant contact area and to measure the *I*-*V* characteristics in wide temperature range. However, the structure of the microfluidics has not been well-optimized, so that the yield of the process has not been improved. Therefore, we propose new fabricating method and the structure of the liquid metal microfluidics.

3. Results and discussion

Fabrication of Bottom Electrode and OSC Ultrathin Film

To prevent short between top and bottom electrode, the roughness of the bottom electrode should be suppressed sufficiently smaller than the thickness of the OSC molecular layer (5.3 nm). We used template strip method [5] to obtain flat electrode with R_a~1 nm. First, we evaporated 200 nm Au onto 6 inch Si wafer with 100-nm-thick thermally oxidized layer in vacuum evaporator (Fig. 5a). Then we mounted glass plates on the Au layer by using optical adhesive (Norland 63) as adhesion layer. After photo-curing of optical adhesive with UV light for 20 min, Au film was peeled off from Si wafer (Fig5b). The obtained Au film showed very small roughness as R_a~0.6 nm (Fig. 5c).

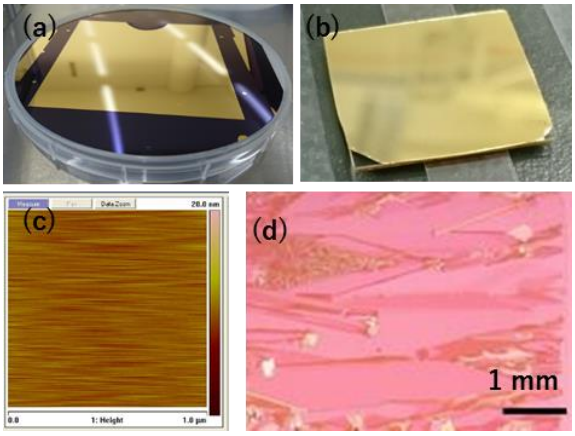

Figure 5 (a) Au film deposited on Si wafer. (b) Template stripped Au film on grass substrate. (c) AFM topography of template stripped Au film. (d) Optical image of Ph-BTBT-C10 coated on template stripped Au.

On the template stripped Au layer, we fabricated OSC single-crystalline films

with blade coating technique by using 0.1 wt% solution of Ph-BTBT-C10 in chlorobenzene. We confirmed the obtained OSC films showed same morphology as the previously reported films: they had two-molecular-layer-unit (5.3 nm) step and terrace structure. We also succeeded in fabricating single molecular bilayer film [6].

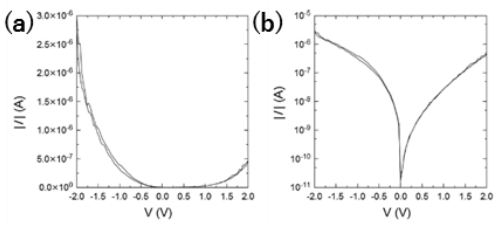

Figure 6 *I-V* characteristics of interlayer transport in (a)linear scale and (b) semi-log scale.

Preliminary Experiment with EGaIn

Before fabricating microfluidic electrode, we confirmed that EGaIn worked as non-invasive electrode material. High surface tension of EGaIn prevent us from drop casting it on OSC film. Instead, we used probe needle coated with EGaIn as top electrode. Figure 6 shows the *I-V* characteristics of interlayer transport in Ph-BTBT-C10. As we previously proposed, obtained *I-V* characteristics showed strong nonlinearity. Asymmetric characteristics against voltage would originate from the asymmetry of electrode work function (EGaIn: 4.3 eV, Au: 5.1 eV). However, this asymmetry is not consistent with other measurement. A failure of thickness determination based on atomic force microscope (AFM) also complicate the interpretation of this experiment.

Fabrication of the 3D mold using the two step DRIE

Figure 7 shows the proposed process flow of the bottom channel in the 3D microfluidics.

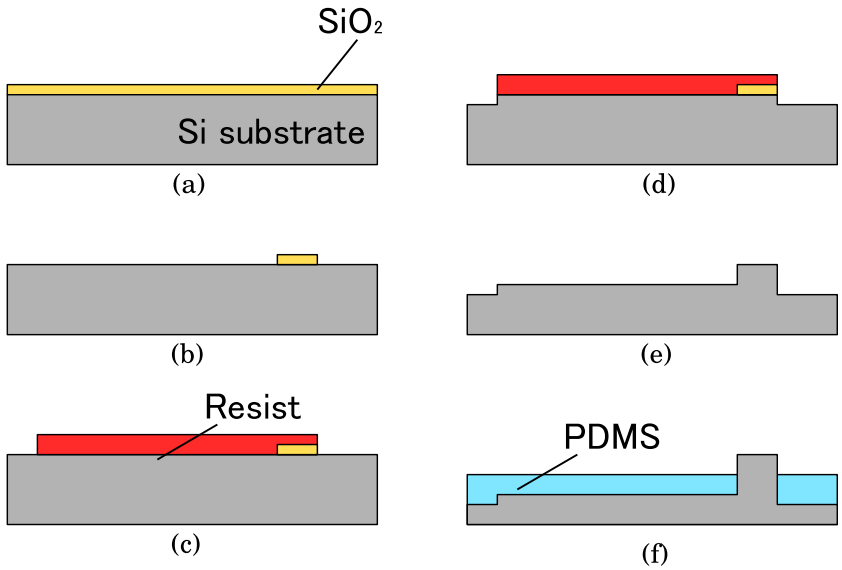

Figure 7. Process flow of the mold of the bottom layer. (a) Silicon wafer is thermally oxidized. (b) The SiO_2 is patterned. (c) The photoresist is patterned. (d) The first DRIE is performed to form the bottom channel, and the resist is stripped. (e) The second DRIE is performed to form the fluidic via. (e) PDMS is poured on the mold and cured.

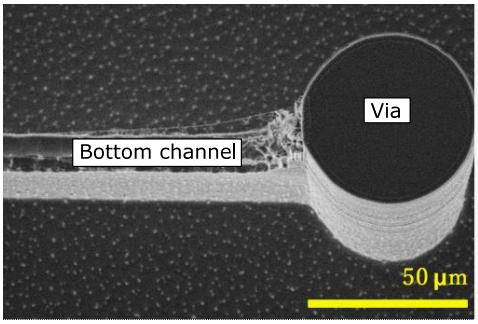

Figure 8. SEM Image of the mold of the bottom layer using two step DRIE.

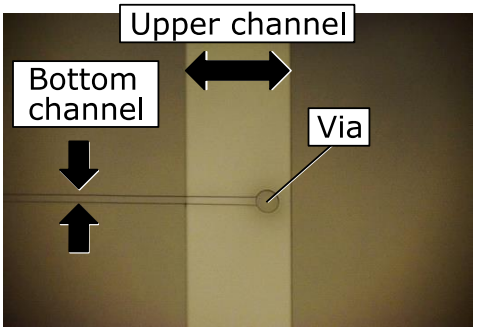

Figure 9. Image of fabricated 3D microfluidics.

Firstly, silicon wafer is oxidized by 500 nm (Fig. 7a). Then, the SiO_2 layer is patterned for the fluidic via (Fig. 7b). After that, the thick 1.5 μm resist is patterned for the bottom micro channel. Subsequently, deep reactive ion etching (DRIE) of silicon is performed by 40 μm to form the bottom micro channel. (Fig. 7d) After the resist is stripped using O_2 plasma, the second DRIE is performed by 50 μm (Fig. 7e). Finally, PDMS is poured on the mold and thermally cured (Fig. 7f). Figure 8 shows the scanning electron microscope (SEM) image of the fabricated silicon mold for the bottom channel. From the Fig. 8, the height difference between the via and the channel is larger than 30 μm, which cannot be obtained using the previous method. Figure 9 shows the optical microscopic image of the fabricated 3D microfluids. The upper micro channel, the bottom micro channel, and the fluidic via can be observed.

Liquid Metal Microfluidics Having Single Layer

As we described in the previous section, we proposed and demonstrated the new fabricating method of the 3D mold using DRIE. Although the proposed method allows us to increase the yield of the fabrication of the bottom micro channel, the uncertainty of bonding of two layers remains. This bonding sequence is another largest reason of degrading the yield and increases the number of fabricating steps. Therefore, we investigated the possibility of single layer microfluidic device for liquid metal. If it is possible to fabricate the liquid metal microfluidics in a

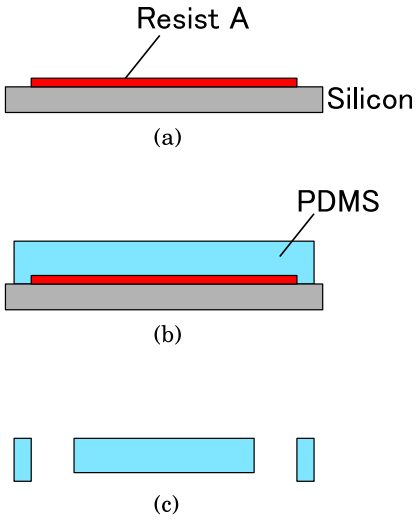

Figure 10. Process flow of the single layer liquid metal microfluidics. (a) The photoresist is patterned. (b) PDMS is poured and cured. (c) PDMS is stripped from the mold and holes are made.

single layer, it allows us to decrease the fabricating steps and improve the yield. In the previous liquid metal microfluidics, inlet to introduce the liquid metal, and outlet to degas, and contact area to a DUT were put separately. This design caused the 3D complex structure. However, the inlet and the contact area can be shared if the size of the real contact can be stabilized. In this research, we proposed new single layer liquid metal microfluidics shown in Fig. 11. We intentionally increase the fluidic resistance by shrinking the size of the microchannel to fix the position of the liquid metal. The microchannels are only used to degas. To prove our concept, we fabricated three devices having different microfluidics. One has a single microchannel, whose height was 50 μm and the width was 1 mm, respectively. Another device has a single microchannel, whose height was 25 μm and the width was 1 mm. The last device has 7 parallel micro channels, whose height was 25 μm and width is 200 μm.

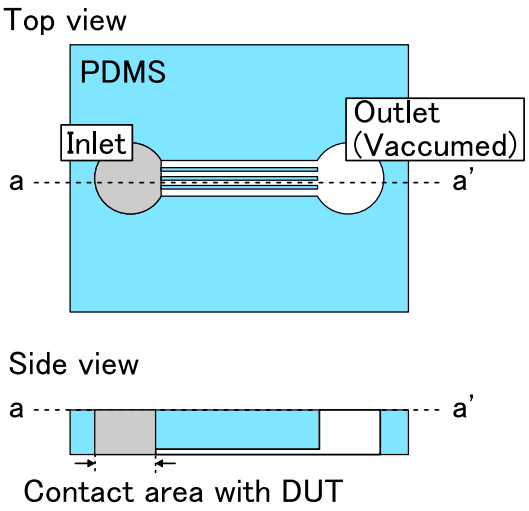

Figure 11. Schematic of proposed single layer liquid metal microfluidics. Microchannel are used only to degas and liquid metal is fixed in the inlet hole.

Introducing Liquid Metal to the 3D Microfluidics Fabricated by the Two Step DRIE

Figure 12 shows the fabricated 3D microfluidics when we introduced the liquid metal (EGaIn). In this structure, the liquid metal did not reach to the bottom channel. This is because the air bubble interrupted the liquid metal from going. The other issue is that the liquid metal flowed only the upper channel when the vacuuming force to degas was too strong. To solve these issues, the another microchannel should be put to degas the air in the bottom micro channel or decrease the fluidic resistance of the bottom micro channel for the liquid metal to go to the bottom channel more smoothly. The adjusting the vacuuming power should be also adjusted.

Introducing Liquid Metal to the Fabricated Single Layer Microfluidics

To confirm the degassing microchannel is really required, we firstly observed a PDMS sheet with a single hole (diameter Φ=1-1.5 mm). After the PDMS sheet is attached to a silicon wafer, we injected the liquid metal (eutectic gallium indium: EGaIn) into that hole. As shown in Fig. 13, EGaIn did not go inside the hole. It is because the air remained, and it interrupted EGaIn.

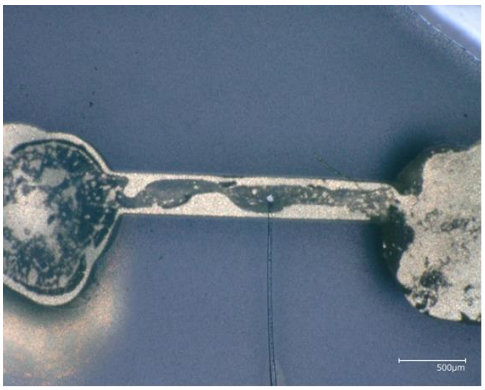

Figure 12. Image of the 3D microfluidics after EGaIn was injected. EGaIn does not flow in the bottom micro channel.

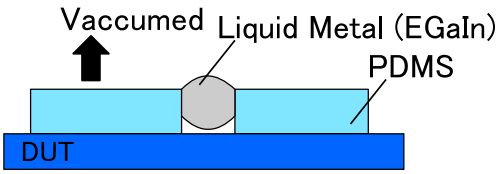

Figure 13. Schematic of the liquid metal on the single hole in a PDMS sheet. Because of the inside air, the liquid metal does not flow inside the hole.

Next, we measured the single channel (height h = 50 µm, width w = 1 mm) microfluidic device. Φ of the inlet and the outlet is the same as the previous experiment. The microfluidics was attached to the silicon wafer. EGaIn was introduced from the inlet. In this device, the liquid metal penetrated up to the silicon wafer without degassing. From the experiment, we consider that the important things to introduce the liquid metal successfully are i) EGaIn is in contact with silicon, which has larger surface energy than PDMS. ii) preparing the air degassing path. Then, the degas was performed using a rotary pump from the outlet. As Fig. 14 a, the liquid metal flowed in the micro channel. Subsequently, we measured the single channel (h = 25 µm, w = 1 mm)

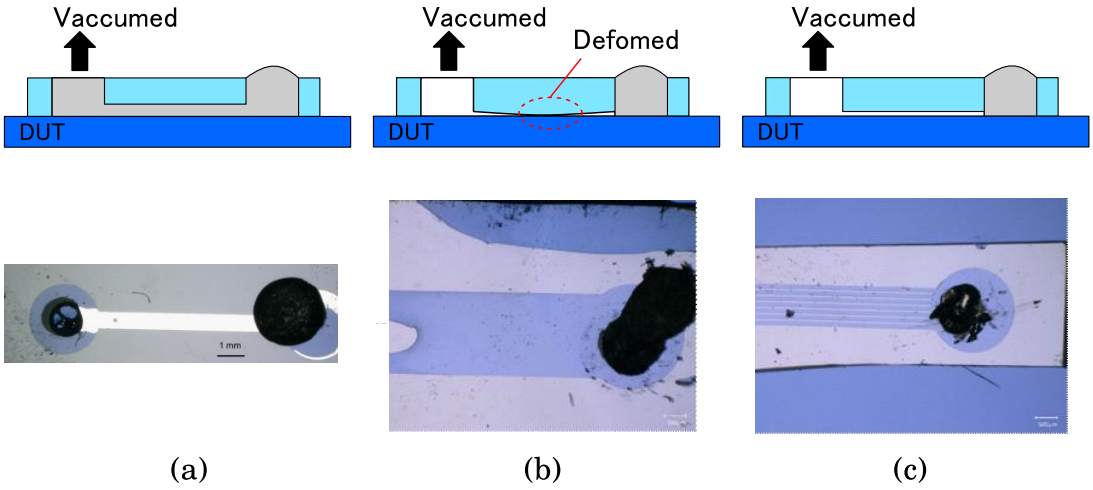

Figure 14. (a) Measurement with the single channel (h = 50 µm, w = 1 mm) microfluidics. Liquid metal is easily penetrated, but it flowed even in the micro channel. (b) Measurement with the single channel (h = 25 µm, w = 1 mm) microfluidics. PDMS deformed and worked as a valve. As a result, the liquid metal is blocked. (c) Measurement with shallow microchannels device (h = 25 µm, w = 200 µm). The liquid metal does not flow in the micro channel because of the high fluidic

microfluidic device and shallow microchannels device (h = 25 μm, w = 200 μm). In both devices, we confirmed the liquid metal did not flow in the microchannels even when the degas was performed from the outlet as shown in Fig. 14b and 14c. In Fig. 14b, the liquid metal flow was blocked by the deformed PDMS, which worked as a physical valve. In Fig. 14c, the narrow microchannels had high fluidic resistance and it blocked only liquid metal.

Electrical Measurement Using Microfluidic Electrode

We measured interlayer transport of single molecular bilayer and 4-bilayer film of Ph-BTBT-C10 using microfluidic electrode. We chose single layer microfluidics with inlet hole filled with EGaIn. All measurement of single molecular bilayer failed due to short between top and bottom electrode. We considered probable origin of short; scratching OSC film with PDMS during transfer, migration of metal atom into OSC film, dissolution of OSC film due to Joule heating. *I-V* characteristics of 4-bilayer device is shown in Fig. 14. It showed nonlinear *I-V* characteristics and was consistent with tunneling transport mechanism inside alkyl chain layer. Simmons equation of tunneling current, which is based on WKB approximation [7], suggests that when an applied voltage V and the tunnel barrier height φ satisfy the relation $eV<<\varphi$, the tunnel current should be proportional to applied voltage ($I \propto V^1$). Actually, the log-log plot (Fig. 15c) fulfilled $I \propto V^1$ for V<0.2 V. However, we did not analyzed the data based on Simmons equation further because the multiple insulating layer based on alkyl chains hindered the modeling of carrier transport.

Here we analyzed the *I-V* characteristics based on single-level model [8]. This model has two assumption: the carrier transport in alkyl chain layer is dominated by 1-dimensional transport in rod-shaped molecules, and only the HOMO level of the alkyl chains is involved in transport. Single-level model formulate the conduction with ε_h, the energy difference between the electrode work function and HOMO of the molecule, Γ, the average interface coupling, and N, the number

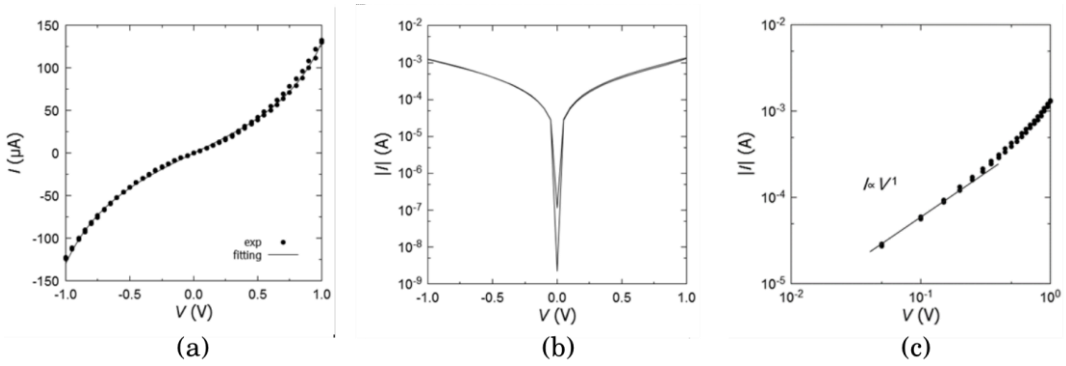

Figure 15 Interlayer *I-V* characteristics of 4-bilayer film of Ph-BTBT-C10 in (a) linear scale, (b) semilog scale, and (c) log-log scale. The solid curve in (a) shows Eq. (1) with N=6.4, ε_h=0.75 eV, Γ=0.78 meV.

of the molecules participating in the transport as

$$I = NG_0 \frac{\Gamma^2}{\varepsilon_h^2 - (eV/2)^2} V \quad (1)$$

where $G_0 = 2e^2/h$ denotes the quantized conductance. The solid line in Fig. 14a shows the fitting curve with Eq. (1). Fitting parameters were calculated as N=6.4, ε_h=0.75 eV, Γ=0.78 meV. The value of ε_h in this experiment would include underestimate: $\varepsilon_h \simeq 1.0$ eV were reported for alkanethiols [8] and we also estimated the barrier height as around 1.0 eV with numerical calculation based on WKB-based model [9]. Besides, N and Γ, which are related to the absolute value of current, are extremely small compared to previous reports. The unexpectedly small values could be interpreted as large contact resistance of chain-chain carrier hopping, and small effective contact area compared to geometrical contact area [10]. However, the single-level model was originally defined for single tunnel junction, so this model might not be appropriate in our device with multiple tunnel barriers.

4. Conclusion and Outlook

In this work, we fabricated microfluidic-channel-supported liquid metal electrode to measure interlayer transport in Ph-BTBT-C10 ultrathin films. Narrowing microchannel enabled the inlet hole to degas without negative pressure and keep the constant contact area. Our new process succeeded in fabricating microfluidic electrode with single layer microfluidics. The electrical measurement of 4-bilayer device showed tunneling transport with extremely large contact resistance. By measuring interlayer transport in ultrathin films with other layer number, especially monolayer film, we would confirm the validity of the measurement and the interpretation reported here. Also, when we will succeed in measuring the interlayer transport in wide temperature range, we will be able to obtain the better understanding of the carrier transport mechanism.

Acknowledgements

We would like to thank the supports and encouragement of our supervisors, Prof. Tatsuo Hasegawa, Prof. Yoshio Mita, Prof. Kazushi Kanoda, and Prof. Takehiko Kitamori. We also thank the MERIT program for providing us the valuable chance of carrying out this interdisciplinary research

References

[1] T. Hamai, *et al.*, *Phys. Rev. Appl.*, **8**, 054011 (2017).

[2] S. Inoue, *et al.*, *Chem. Mater.*, **27**, 3809 (2015).

[3] A. C. Dürr, *et al.*, *J. Appl. Phys.*, **93**, 5201 (2003).

[4] A. Wan, *et al.*, *Adv. Funct. Mater.*, **24**, 4442-4456 (2014).

[5] E. A. Weiss, *et al.*, *Langmuir*, **23**, 9686-9694 (2007).

[6] S. Arai, *et al*., *Adv. Mater*., **30**, 1707256 (2018).
[7] J. G. Simmons, *J. Appl. Phys.*, **34**, 1793 (1963).
[8] Z. Xie, *et al.*, *ACS Nano*, **11**, 569-578 (2017).
[9] T. Hamai, *et al.*, *J. Mater. Res.*, **33**, 2350-2363 (2018).
[10] F. C. Simeone, *et al.*, *J. Am. Chem. Soc.*, **135**, 18131-18144 (2013).